Since January 2020 Elsevier has created a COVID-19 resource centre with free information in English and Mandarin on the novel coronavirus COVID-19. The COVID-19 resource centre is hosted on Elsevier Connect, the company's public news and information website.

Journal of Functional Foods 75 (2020) 104282

Contents lists available at ScienceDirect

Journal of Functional Foods

journal homepage: www.elsevier.com/locate/jff

The potential antiviral effect of major royal jelly protein2 and its isoform X1 against severe acute respiratory syndrome coronavirus 2 (SARS-CoV-2): Insight on their sialidase activity and molecular docking

Noha H. Habashy [a,*], Marwa M. Abu-Serie [b]

[a] Biochemistry Department, Faculty of Science, Alexandria University, Alexandria 21511, Egypt
[b] Department of Medical Biotechnology, Genetic Engineering, and Biotechnology Research Institute, City for Scientific Research and Technology Applications (SRTA-City), New Borg EL-Arab 21934, Alexandria, Egypt

ARTICLE INFO

Keywords:
SARS-CoV-2
Major royal-jelly protein (MRJP) 2
MRJP2 isoform X1
Sialidase
In-silico analysis

ABSTRACT

Severe acute respiratory syndrome-coronavirus (SARS-CoV)-2 is a newly emerging type of CoV. We evaluated the predicted anti-SARS-CoV-2 effect of major royal jelly protein (MRJP)2 and MRJP2 isoform X1, which recently showed high efficacy against other enveloped RNA-viruses (HCV and HIV). Some in-silico analyses have been performed to predict the impact of these proteins on viral entry, replication, and complications. These proteins have shown a high potency in sialic acid hydrolysis from the lung cells (WI-38) surface. Docking analysis showed that these proteins have a high binding affinity to viral receptor-binding sites in the receptor-binding domain, causing attachment prevention. Moreover, MRJPs can exert an inhibitory influence, via different mechanisms, for SARS-CoV-2 non-structural proteins (main and papain proteases, RNA replicase, RNA-dependent RNA polymerase, and methyltransferase). Also, they can bind to hemoglobin-binding sites on viral-nsps and prevent their hemoglobin attack. Thus, MRJP2 and MRJP2 X1 can be a promising therapy for SARS-CoV-2 infection.

1. Introduction

Since the end of 2019 to the present, severe acute respiratory syndrome coronavirus 2 (SARS-CoV-2) has caused widespread infection and is considered a threat to public health security. CoVs (7 species) have a positive-sense single-strand RNA genome with an envelope protein containing a spike protein. The latter protein forms a sun-like morphology that gives this virus its Latin name—"corona" (crown or halo) (Bassetti, Vena, & Giacobbe, 2020; Tok & Tatar, 2017). SARS-CoV-2 belongs to the Nidovirales order, the Coronaviridae family, the Coronavirinae subfamily, and the bat coronavirus genus (β-CoVs), which mainly affects the respiratory tract of animals and humans (Chan et al., 2020). Beside SARS-CoV-2, two highly pathogenic β-CoVs (the SARS-CoV outbreak in 2002 and the Middle East respiratory syndrome "MERS-CoV" outbreak in 2012) have been documented. Zoonotic β-CoVs (SARS-CoV-2, SARS-CoV, and MERS-CoV) emerged from bats and were transmitted to humans, causing typical pneumonia, respiratory failure, and death (Chan et al., 2020; Cui, Li, & Shi, 2019). Based on WHO data, 2229 patients with MERS-CoV (35.5% mortality) and 8422 patients of SARS-CoV infections (9.6% mortality) were reported worldwide (WHO, 2004, 2019). In Wuhan, China (29th December 2019), the first four cases of SARS-CoV-2 were reported in workers in the South China seafood wholesale markets (Chinese Center for Disease Control and Prevention, 2020). Outside China, SARS-CoV-2 has spread till now (October 5, 2020) to 235 countries, areas or territories, and there are more than 35 million confirmed cases and more than one million confirmed deaths. These patients exhibit symptoms of acute lung syndrome known as the coronavirus disease (COVID) 2019 (WHO, 2020).

SARS-CoV-2 (29891 nucleotides) is closer to SARS-CoV (29751 nucleotides) in terms of gene sequence, encoded proteins, and behavior patterns than to MERS-CoV (Bassetti et al., 2020; Chan et al., 2020). Thus, certain therapeutic strategies could be relevant to both groups of viruses (Chen, Liu, & Guo, 2020; Gorbalenya, 2020). Two-thirds of their genomes encode polyproteins 1a and 1ab that generate 16 non-structural proteins (including the RNA replicase-transcriptase complex) via 3-chymotrypsin-like protease (3CL) cleavage. The remaining genome encodes accessory proteins and four structural proteins, including nucleocapsid (N), membrane (M), envelope (E), and spike (S). Certain position in the latter, which are named receptor-binding domain

* Corresponding author.
E-mail address: noha.Habashi@alexu.edu.eg (N.H. Habashy).

https://doi.org/10.1016/j.jff.2020.104282
Received 17 July 2020; Received in revised form 3 November 2020; Accepted 7 November 2020
Available online 11 November 2020

(RBD), binds to the angiotensin-converting enzyme (ACE)2, mediating viral entry and replication in the cytoplasm (Chan et al., 2020; Letko & Munster, 2020). Such SARS-CoVs can then invade the lung cells and cause downregulation of ACE2, thereby leading to an abnormal level of angiotensin II that increases the pulmonary vascular permeability. In severe cases, SARS-CoVs evade immune surveillance and induce an uncontrolled inflammatory response (inflammatory cell infiltration with a massive production of proinflammatory cytokines). All of these disorders eventually deteriorate into pulmonary edema and respiratory distress with organ damage (Li et al., 2020; Xu et al., 2020).

To date, no clinical medication (therapy or vaccines) has been developed for the new emerging SARS-CoV-2. Since CoV is an enveloped RNA virus, a human immunodeficiency virus (HIV) and hepatitis C virus (HCV) treatment strategy could be applied. Recent results of modelling and molecular docking have predicted that Tenofovir (anti-HIV drug) and Sofosbuvir (anti-HCV drug) are active against SARS-CoV-2 (Elfiky, 2020). In our recent studies, the purified major royal jelly proteins (MRJPs) of *Apis mellifera* was shown to exhibit powerful antiviral activity against HCV and HIV (EL-Fiky, Abu-Serie, & Habashy, 2018, 2020; Habashy & Abu-Serie, 2019). RJ is a superfood secreted from the mandibular and hypopharyngeal salivary glands of young nurse bees aged 5–14 days. It is a unique nutrient for all larvae in the first three days, but only the queen bees feed on it all their lives (Fratini, Cilia, Mancini, & Felicioli, 2016). RJ is a functional food with antimicrobial, anti-aging, antioxidant, and immunomodulatory effects, as well as other health benefits for diabetes, cancer, Alzheimer's, and cardiovascular disease (Ahmad, Campos, Fratini, Altaye, & Li, 2020). These activities are related to the several functional constituents of RJ, such as proteins, lipids, carbohydrates, vitamins, and minerals, among others (Fratini et al., 2016). The majority of RJ proteins (about 90%), comprising nine members (MRJP1-MRJP9), are water-soluble and have many physiological functions (Albert, Bhattacharya, Klaudiny, Schmitzová, & Simúth, 1999; Scarselli et al., 2005; Šimúth, Bíliková, Kováčová, Kuzmová, & Schroder, 2004). Among these MRJPs, we have recently proven the antiviral, anticancer, and anti-hepatic damage potential of MRJP2 and MRJP2 X1 (Abu-Serie & Habashy, 2019; Habashy & Abu-Serie, 2019). In this study, in prolongation of our recent work, the possible inhibitory effect of these two functional food components, MRJP2 and MRJP2 X1, on SARS-CoV-2 was investigated using some *in silico* analyses.

2. Methods

2.1. Chemicals

Polyacrylamide, carboxymethyl (CM)-Sephadex, sialic acid (SA), and 3-(4,5-dimethylthiazol-2yl-)-2,5-diphenyl tetrazolium bromide (MTT) were obtained from Sigma-Aldrich (St. Louis, MO, USA). Ammonium sulfate was supplied from Nentech Ltd (NTL, Brixworth, Northants, UK). Dulbecco's Modified Eagle's medium (DMEM) and fetal bovine serum (FBS) were obtained from Lonza (USA). Protease inhibitor cocktail (PIC) was obtained from Thermo Scientific, USA. Human normal lung fibroblast WI-38 cell line was purchased from the American Type Culture Collection (ATCC, USA). Other chemicals were obtained with a high grade.

2.2. Purification of MRJP2 and its isoform X1

The RJ was obtained from the local market in Egypt and used instantly for the purification of MRJP2 and MRJP2 X1 following our preceding method (Abu-Serie & Habashy, 2019). In brief, the non-soluble proteins were discarded via centrifugation at 3800*g*, 30 min, and 4 °C. Then the protein fraction 50 (PF_{50}) was precipitated (3800*g*, 30 min, and 4 °C) by ammonium sulfate at 40–50% saturation. After dialysis (24 h, 4 °C) against the binding buffer (20 mM phosphate buffer containing 1x PIC, pH 6.7), MRJP2 and its isoform X1 were purified using the CM-Sephadex ion-exchange column chromatography at 4 °C. The dialysate was applied to the column, and the unbound MRJP2 X1 (yield ~ 1.30 g%) was collected first. The elution buffer was a binding buffer comprising 0.5 M NaCl and was used to collect the bound MRJP2 (yield ~ 1.54 g%). Both MRJP2 and its isoform X1 were dialyzed for 24 h at 4 °C against PBS (pH 7) and then lyophilized (Telstar, Terrassa, Spain) and kept at −80 °C until used.

2.3. Determination of sialidase activity of RJ proteins

The sialidase catalytic activity of MRJP2 and MRJP2 X1 was assessed using the human normal lung fibroblast WI-38 cell line.

2.3.1. Cytotoxicity of RJ-PFs on human normal lung cells

The human normal lung fibroblast WI-38 cell line was subcultured in DMEM medium—containing 10% FBS—seeded at 3×10^3 cells per well in a 96-well cell culture plate and incubated for 24 h at 37 °C in a 5% CO_2 incubator. Serial concentrations of the studied proteins (MRJP2 X1, MRJP2, and PF_{50}) were added to the attached cells. After 72 h of incubation, cell viability was assessed by the MTT method (Mosmann, 1983). Twenty microliters of 5 mg/mL MTT were added to each well, and the plate was incubated at 37 °C for 3 h. Then the MTT solution was removed, 100 μl DMSO was added, and the absorbance was measured with a microplate reader (BMG LabTech, Germany) at 570 nm. The safe dose (EC100, the concentrations being equivalent to 100% cell viability) of the tested proteins was estimated using the GraphPad InStat software.

2.3.2. Sialidase activity assay

Different concentrations (5.000, 2.500, 1.250, 0.625, and 0.315 mg/mL) of each PF were incubated with WI-38 cells at 37 °C for 2 h. Moreover, different concentrations of MRJP2 (4.00, 2.00, 1.00, 0.50, and 0.25 mg/mL), MRJP2 X1 (0.500, 0.250, 0.125, 0.062, and 0.031 mg/mL), and PF_{50} (1.500, 0.750, 0.375, 0.187, and 0.094 mg/mL) were incubated with WI-38 cells for 72 h. Three controls were included: PF alone without cells, cells without PF (negative control), and cells exposed to 2 M acetic acid for 2 h at 80 °C (total amount of cellular SA, positive control "C"). At the end of the incubation period, cell cultures were centrifuged at 2000 rpm for 15 min, and the released SA was quantified in the supernatant through the alkali-Ehrlich method (Aminoff, 1961). The concentration of SA (nmol/mL) was determined by the standard SA calibration curve and was used to calculate the sialidase activity of each RJ-PF in terms of nmol/ml/min (IU). The specific activity (IU/mg of protein) was calculated after measuring the protein content (mg/mL) in the cell culture supernatant using the Bradford method (Bradford, 1976); it was then divided by the positive control value (C) to get the % activity. The EC50 values (concentrations equivalent to 50% activity) were calculated by fitting a sigmoidal dose–response curve (variable slope) using the GraphPad PRISM program (version 6) with an appropriate 95% confidence interval.

2.4. MRJP2 and MRJP2 X1 combination study

The effect of MRJP2 and MRJP2 X1 combination (PF_{50}) on the sialidase activity has been studied. This combination can confer lower (antagonistic), higher (synergistic), or no change (additive) in this catalytic activity. The probable new effect was evaluated by the effect "Fa"-combination index (CI) plot as well as the CI at different Fa values (0.5, 0.75, and 0.9) using the CompuSyn software (Chou, 2006).

2.5. In silico analyses

2.5.1. 3D protein modelling

The 3D structure of the SARS-CoV-2 proteins was obtained from the Protein Data Bank (PDB) (https://www.rcsb.org/). These proteins encompassed papain-like protease (non-structural protein nsp3, PDB: 6WUU), 3CL protease (nsp5, PDB: 6WTT), nsp5-inhibitor complex (PDB:

7BRP), and RNA replicase (nsp9, PDB: 6WXD). Also, RNA-dependent RNA polymerase (nsp12)-cofactor (nsp7-nsp8) complex (PDB: 7BV2) and methyltransferase (nsp16)-cofactor (nsp10) complex (PDB: 6YZ1) were involved. Moreover, ACE2-RBD (PDB: 6M0J), ACE2-inhibitor complex (PDB: IR42), human oxy-hemoglobin (PDB: 6BB5), and human deoxyhemoglobin (PDB: 1A3N) were extracted from the PDB database. The 3D structure of proteins that did not have any structural models in the PDB was predicted from its amino acid sequence that had been obtained from the NCBI protein database(https://www.ncbi.nlm.nih.gov/protein/). This was achieved using the Iterative Threading ASSEmbly Refinement (I-TASSER) protein-modelling online platform (http://zhanglab.ccmb.med.umich.edu/I-TASSER/) (Yang & Zhang, 2015). Such proteins comprise the two purified *A. mellifera* proteins, MRJP2 (**Accession**: ACS66837, 452 amino acids) and MRJP2 X1 (**Accession**: XP_026299315, 452 amino acids). Based on the predicted I-TASSER structures, the functional predictions of MRJP2 and MRJP2 X1 were deduced from the COFACTOR (https://zhanglab.ccmb.med.umich.edu/COFACTOR/) (Zhang, Freddolino, & Zhang, 2017) and COACH (https://zhanglab.ccmb.med.umich.edu/COACH/) (Yang, Roy, & Zhang, 2013) servers.

2.5.2. Active site identification

The active site residues in the studied viral enzymes were accessed from the PDBsum web-based database (http://www.biochem.ucl.ac.uk/bsm/pdbsum) (Laskowski, Jabłońska, Pravda, Vařeková, & Thornton, 2018) using the protein PDB ID. This web server provides structural data on inputs in the PDB database.

2.5.3. Molecular docking

The predicted 3D structure models of MRJP2 and MRJP2 X1 with the highest C-score were docked individually with viral proteins (nsp3, nsp5, nsp9, nsp12, nsp12-nsp7-nsp8, nsp16, nsp16-nsp10, and RBD), ACE2, and SA to acquire the structural complexes.

To better understand the possibility of MRJP2 or MRJP2 X1 interacting with SARS-CoV-2 proteins, protein–protein docking was performed using the GRAMM-X Protein Protein Docking Server (http://vakser.compbio.ku.edu/resources/gramm/grammx/) (Tovchigrechko & Vakser, 2006). The chemical structure of N-acetylneuraminic acid "NeuAc" (PubChem CID: 439197) and 9-O-acetyl SA (PubChem CID: 123962) was obtained from the PubChem compound database. Then it was docked with each of the studied RJ-PFs via the PatchDock web server (https://bioinfo3d.cs.tau.ac.il/PatchDock/php.php) using the default value of the clustering RMSD, i.e., value = 4 (Schneidman-Duhovny, Inbar, Nussinov, & Wolfson, 2005). Of all the structural complexes obtained, the one with the highest score was selected for further analysis.

2.5.4. Analysis of the docked complexes

Certain computational analyses were performed to characterize the docking properties of MRJP2 and MRJP2 X1 with SARS-CoV-2 proteins. The generated structural complexes were further refined by the FireDock (Fast Interaction Refinement in the molecular Docking) server (http://bioinfo3d.cs.tau.ac.il/FireDock/php.php) (Mashiach, Schneidman-Duhovny, Andrusier, Nussinov, & Wolfson, 2008). This analysis was used to re-score the docked complexes based on their global (binding) energy.

Moreover, the interchain interactions in docked protein complexes were studied through the PIMA (Protein-Protein Interactions in Macromolecular Assemblies) server (http://caps.ncbs.res.in/pima/) (Mathew & Sowdhamini, 2016). This tool provided information about the total number of atoms in each chain, interface residues, van der Waals pairs, hydrophobic, salt bridge, and favorable and unfavorable electrostatic interactions.

The docked structural complexes were visualized and analyzed via the Discovery Studio 2017 R2 software and the Protein-Ligand Interaction Profiler (PLIP) tool (https://projects.biotec.tu-dresden.de/plip-web/plip/index) (Salentin, Schreiber, Haupt, Adasme, & Schroeder, 2015) to identify the binding pocket atoms and the 2D diagram of the MRJPs–SA interactions. Furthermore, the binding affinity of the MRJPs–SA docked complexes was identified using the atomic contact energy value (ACEV) provided by the PatchDock server and the fullfitness value was obtained from the SwissDock web service (http://www.swissdock.ch/) (Grosdidier, Zoete, & Michielin, 2011).

2.6. Statistical analysis

Results were presented as mean ± SE and analyzed via the SPSS version 16. One-way analysis of variance (ANOVA) was used to compare mean values through Duncan's test, and the significance was set at $P < 0.05$. The GraphPad InStat software version 3 was used to calculate EC100 values, and the GraphPad Prism version 6 was used to calculate EC50 values. The CompuSyn software (ComboSyn, Inc., Paramus, NJ) generated CI plots and values for SA results.

3. Results

3.1. 3D structures and sialidase activity of MRJP2 and MRJP2 X1

The RJ-PF_{50} was fractionated, on the CM-Sephadex ion-exchange column, into two proteins: MRJP2 and MRJP2 X1. A single characteristic band of each protein, with a molecular mass of nearly 49.95 kDa and 53.12 kDa, respectively, was observed via sodium dodecyl sulfate–polyacrylamide gel electrophoresis (SDS-PAGE) (Abu-Serie & Habashy, 2019; Habashy & Abu-Serie, 2019). The predicted 3D structure of each purified protein was obtained from the most ranked server, I-TASSER. The 3D structure model with the highest C-score value (model 1) was used for further analyses. Certain predicted molecular, biological, and cellular functions of the two purified RJ proteins were observed using COFACTOR and COACH computational methods. These analyses revealed that the top-ranked template proteins in the PDB with similar binding sites to MRJP2 (4HIZA, 2AGSA, 1S0KA, 1VUB, 2F10A, 1EUUA, 3GVJ, and 1V0EA) and MRJP2 X1 (4HIZA, 2AGSA, 1S0KA, 1VUB, 2F10A, and 1EUUA) are sialidases. Therefore, the two purified RJ proteins were tested for sialidase activity using WI-38 cells and different concentrations of RJ-PFs.

The cytotoxicity study showed that the safe dose values (EC100) for MRJP2 (5.555 ± 0.129) and PF_{50} (5.457 ± 0.105) were the same and superior to those of MRJP2 X1 (5.013 ± 0.012) after 2 h of incubation with WI-38 cells. However, these values were 4.655 ± 0.007, 1.500 ± 0.078, and 0.319 ± 0.004 mg/mL, respectively, at 72 h incubation and were significantly different ($P < 0.05$). The results in Fig. 1 (I, II) show that the incubation of MRJP2 or MRJP2 X1 with WI-38 cells resulted in an increase in SA levels in the culture medium relative to the negative control cells, reflecting the sialidase activity of the studied RJ proteins. In addition, the concentration of liberated SA after 72 h incubation of RJ-PF with lung cells was more than that observed at 2 h (time-dependent) and increased with the rise in the concentration of RJ-PF (concentration-dependent). The EC50 values for MRJP2, MRJP2 X1, and PF_{50} after 2 h and 72 h incubation have been denoted in Fig. 1 (Ii and IIi). The statistical analysis for the EC50 values showed that the ability of MRJP2 to hydrolyze SA from the surface of WI-38 cells was similar to that of PF_{50} and higher than that of MRJP2 X1 during both incubation periods. Concerning the sialidase activity of the MRJP2 and MRJP2 X1 combination (PF_{50}, Fig. 1 III, IV), the CI plot and values revealed a synergistic (CI < 1) effect after 2 h and 72 h of incubation with WI-38. Hence, the values of CI after 2 h of incubation at Fa = 0.5, 0.75, and 0.9 were 0.295, 0.099, and 0.033, respectively, and 0.566, 0.721, and 0.999, respectively, after 72 h of incubation.

Docking analysis was performed between MRJP2 or MRJP2 X1 with NeuAc or 9-O-Ac-SA (Fig. S1 I, II) using the PatchDock web server to recognize the type of interactions and binding affinity (ACEV). Results from the 2D structures (Ligplots) and PLIP server revealed that NeuAc

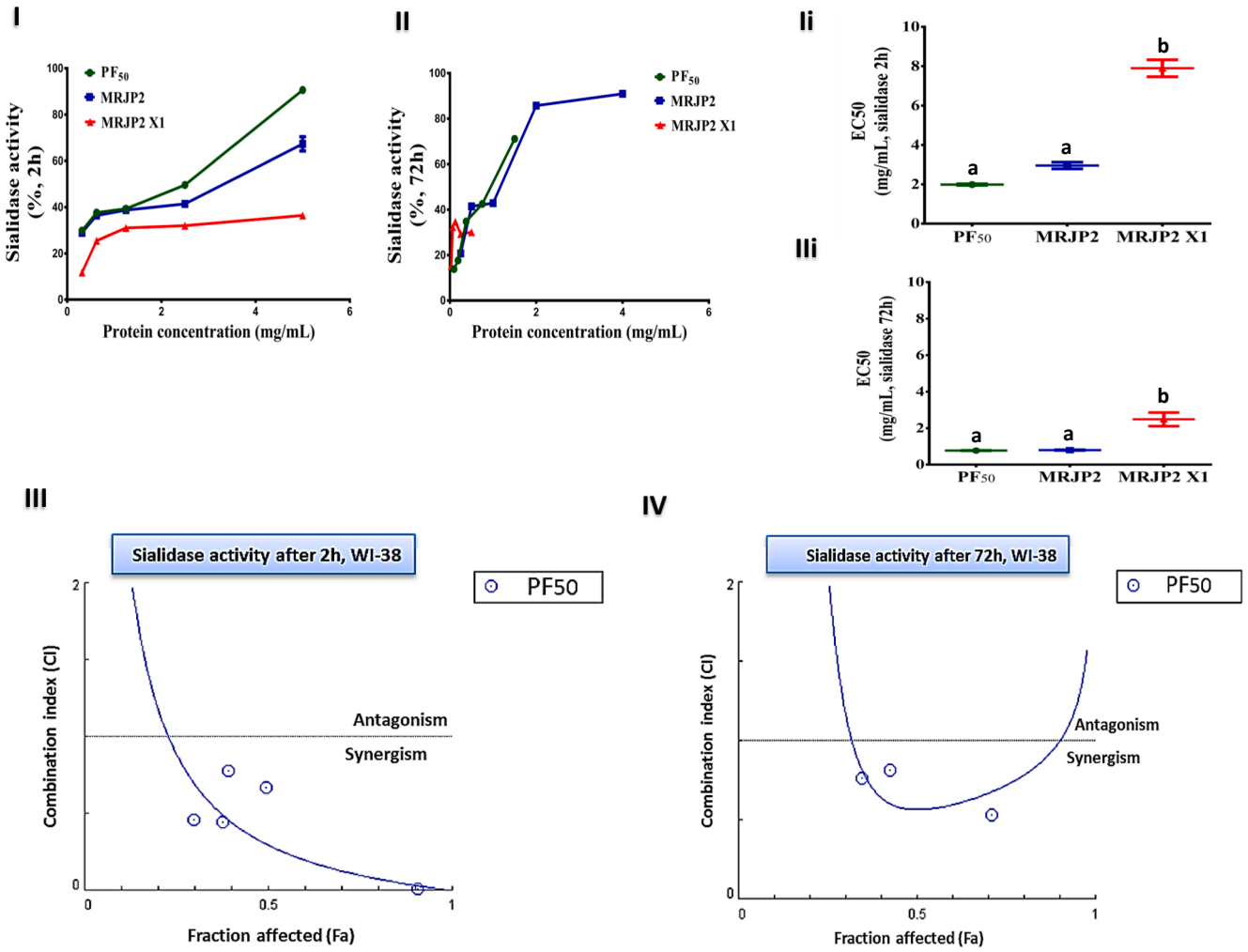

Fig. 1. Sialidase activity of MRJP2, MRJP2 isoform X1, and protein fraction $(PF)_{50}$. ***(I, II)*** Different concentrations of MRJP2, MRJP2 isoform X1, and PF_{50} and their corresponding sialidase activities (%) after 2 h and 72 h incubation with WI-38 cells, respectively. ***(Ii, Iii)*** The EC50 values of the RJ proteins after 2 h and 72 h incubation with WI-38 cells, respectively. Results are presented as mean ± SE (n = 3). Different letters for the same incubation period are significantly different at $P < 0.05$. ***(III, IV)*** Fraction affected (Fa)-combination index (CI) plots used to study the combined (PF_{50}) effect of MRJP2 and MRJP2 X1 on sialidase activity after 2 h and 72 h incubation period, respectively.

interacted with MRJP2 through M254, L256, V309, I357, E360, and L361 through five hydrogen bonds and two hydrophobic interactions (Fig. S1 I, Ii). It interacted with MRJP2 X1 through seven hydrogen bonds, two hydrophobic interactions, and one salt bridge at H62, T63, K64, N65, K39, Y40, F391, F393, N397, and D389 (Fig. S1 III, IIIi). However, the interacting residues between MRJP2 and 9-O-Ac-SA were A255, L256, A308, V309, S310, I357, E360, and L361 via five hydrogen bonds in addition to two hydrophobic interactions (Fig. S1 II, IIi). On the other hand, 9-O-Ac-SA interacted with MRJP2 X1 (Fig. S1 IV, IVi) at L82, K183, H206, D389, and Y66 via three hydrogen bonds, two hydrophobic interactions, two salt bridges, and a covalent bond. The residues mentioned above may serve as the predicted active sites for these new RJ sialidases. The computational methods also revealed the binding affinity (ACEV and fullfitness) of MRJP2 and MRJP2 X1 to NeuAc and 9-O-Ac-SA. The results showed that the ACEV of NeuAc at MRJP2 and MRJP2 X1 were −203.23 and −130.42 Kcal/Mol, respectively. These values were −231.60 and −53.40 Kcal/Mol for 9-O-Ac-SA at MRJP2 and MRJP2 X1, respectively. Moreover, the fullfitness value for MRJP2-NeuAc was −1861.99 Kcal/Mol and that for MRJP2 X1-NeuAc was −1260.60 Kcal/Mol, whereas that value for MRJP2-9-O-Ac-SA and MRJP2 X1-9-O-Ac-SA was −1873.37 and −1266.59 Kcal/Mol, respectively.

3.2. Molecular docking studies for MRJP2, MRJP2 isoform X1, and hemoglobin with SARS-CoV-2 proteins

The present study considered nine proteins, five nsps (nsp3, nsp5, nsp9, nsp12, and nsp16), ACE2 (viral receptor), RBD (spike glycoprotein subunit domain S1), oxy-hemoglobin, and deoxyhemoglobin. All of these proteins were individually docked with MRJP2 and MRJP2 X1. The docked complexes were then analyzed using different computational methods to recognize interchain interactions, binding pockets, and binding energy. The binding pockets in each docked complex (Figs. 2, 3, and S2–S4) were depicted using the CPK "space-filling spheres" style. The global (binding) energy (Kcal/Mol) of MRJP2 with RBD, ACE2, nsp3, nsp5, nsp9, nsp12, and nsp16 were −48.12, −47.98, −49.31, −57.11, −51.36, −50.51, and −38.65, respectively, while this value with nsp12-nsp7-nsp8 and nsp16-nsp10 complexes were −42.19 and −35.86 Kcal/Mol, respectively. In case of MRJP2 X1, these values were −51.12, −33.24, −45.71, −57.30, −21.68, −23.51, −44.85, −24.80, and −56.72 Kcal/Mol, respectively. In addition, Table 1 represents the global energy of binding viral nsps with the human oxy- or deoxyhemoglobin.

The findings in Fig. S2 denote the binding of MRJPs to viral RBD protein (229 amino acids; Fig. S2 III, IV) and chain A of the human ACE2 (603 amino acids; Fig. S2 I, II). Specific types of non-covalent bonds

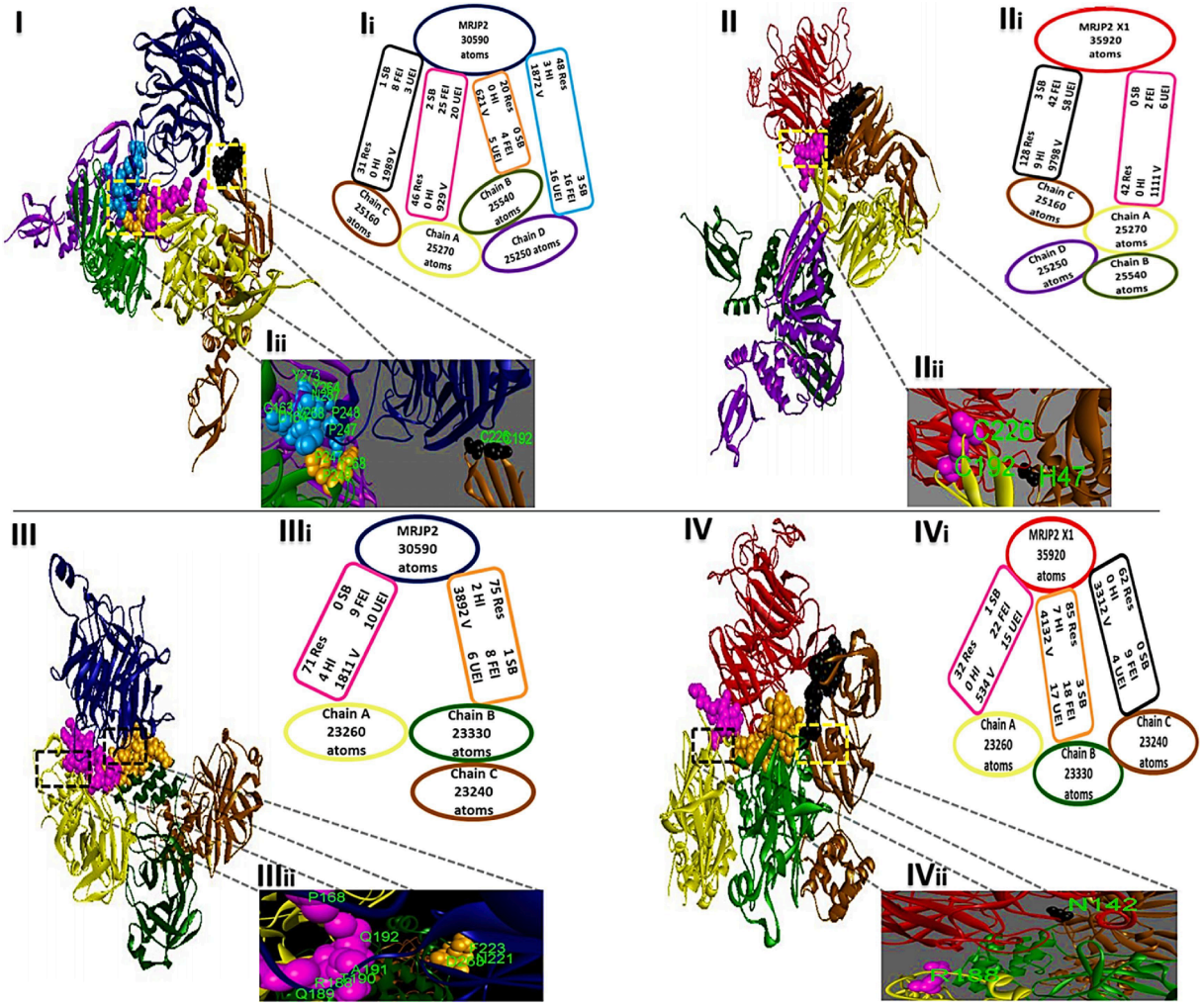

Fig. 2. Molecular docking analysis of MRJP2 and MRJP2 isoform X1 with SARS-CoV-2 nsp3 and nsp5. ***(I, II)*** Docking models of MRJP2 (shown in blue) and MRJP2 X1 (shown in red), respectively with nsp3 (PDB: 6WUU, shown in yellow chain A, green chain B, brown chain C, purple chain D). ***(III, IV)*** Docking models of MRJP2 (shown in blue) and MRJP2 X1 (shown in red), respectively with nsp5 (PDB: 6WTT, shown in yellow chain A, green chain B, brown chain C)**.** The amino acid residues with the space-filling spheres style (shown in pink chain A, orange chain B, black chain C, light blue chain D) indicate the binding residues in the docked complexes. ***(Ii-IVi)*** Illustrations of the interchain interactions (rectangle shapes) in the docked complexes. ***(Iii)*** Magnification of the matched amino acid residues in the nsp3′s active site (Y268B, C192C, C226C, G163D, D164D, P247D, P248D, Y264D, Y268D, and Y273D) and inhibitor binding site (P247B, P248B, Y268B, G163D, D164D, P247D, P248D, Y264D, N267D, Y268D, and Y273D) with MRJP2. ***(IIii)*** Magnification of the nsp3′s active site amino acid residues that can bind with MRJP2 X1. ***(IIIii, IVii)*** Magnification of the matched amino acid residues in nsp5′s active site (Q189A, T190A, Q192A, N221B, F223B, and D263B) or N142C and inhibitor binding site (P168A, R188A, Q189A, T190A, A191A, and Q192A) or R188A, with MRJP2 and MRJP2 X1, respectively. ***Res*** – residues, ***HI*** – hydrophobic interaction, ***V*** – van der Waals, ***SB*** – salt bridge, ***FEI*** – favorable electrostatic interaction, ***UEI*** – unfavorable electrostatic interaction. (For interpretation of the references to colour in this figure legend, the reader is referred to the web version of this article.)

were involved in these interactions (Fig. S2 Ii–IVi), as computed by the PIMA server. Fig. 2 illustrates that nsp3 comprises four polypeptide chains (A, B, C, and D, 326 amino acids) that can interact individually with MRJP2 and MRJP2 X1 via different types of interactions (Fig. 2 Ii–IVi). MRJP2 could interact with all enzymes' polypeptide chains (Fig. 2 I), while MRJP2 X1 could only bind to two chains, A and C (Fig. 2 II). In addition, MRJP2 could bind to all polypeptide chains of SARS-CoV-2′s main protease (nsp5, three polypeptide chains A, B, and C, 310 amino acids) through different types of bonds (Fig. 2 III, IIIi). However, its isoform only interacted with the viral enzymes' chains A and B (Fig. 2 IV, IVi). Fig. 3 shows the docked complexes of purified RJ proteins with nsp9 (116 amino acids, two polypeptide chains A and B, Fig. 3 I, II) or nsp12 (951 amino acids, chain A, Fig. 3 III, IV). Both RJ proteins could interact with nsp9 chain B and nsp12 chain A, while only MRJP2 could bind to the chain A of nsp9 (Fig. 3 Ii–IVi). With respect to the nsp12-nsp7-nsp8 complex (nsp12 chain A, nsp8 207 amino acids, chain B, and nsp7 92 amino acids, chain C), MRJP2 could bind to both chains A (nsp12) and B (nsp8) with different non-covalent interactions (Fig. S3 I, Ii). On the other hand, MRJP2 X1 interacted only with nsp12 and was unable to interact with its cofactor (Fig. S3 II, IIi). These RJ proteins could also bind to chain A of viral nsp16 (chain A, 299 amino acids, Fig. S4 I, II) and the two chains of nsp16-nsp10 (nsp16 chain A and nsp10 "123 amino acids, chain B, Fig. S4 III, IV).

The results in Fig. S5 show that nsp5, nsp9, and nsp16-nsp10 could interact individually with both oxy-hemoglobin chains (Fig. S5 I–III). Concerning the deoxyhemoglobin (Fig. S5 IV-VI), the nsps could interact with one (nsp9), two (nsp16-nsp10), or three (nsp5) chains.

3.3. Analysis of the binding residues in the docked complexes

The active site residues in the studied enzymes (nsp3, nsp5, nsp9, nsp12, nsp16, and ACE2) were extracted from the PDBsum web server and visualized and analyzed through the Discovery Studio program. A comparison between the residues for each tested enzyme and the

Table 1
The global energy of the hemoglobin-non structural proteins (nsps) docked complexes and the matched residues in their binding site with the major royal jelly proteins (MRJPs)-nsps docked complexes.

hemoglobin -SARS CoV-2 nsp complex	Global (Binding) energy (Kcal/Mol)	The nsp binding residues with hemoglobin
Oxy-hemoglobin-nsp5 complex	-44.96	**Chain A** 5K, 133N, 135T, 137K, 138G, 139S, 140F,141L, 166E, ***168P***, ***169T***, 170G, 171V, 172H,***190T***, ***191A***, ***192Q***,***193A***, ***194A***, ***195G***, ***196T***, ***197D***, 199T, 204V, ***236K***, ***237Y***, ***238N***, ***239Y***, 271L, 272L, 273Q, 274N, 275G, 276M, 277N, 278G,284S, 286L, 287L, 288E,289D. **Chain B** ***224T***, ***244Q***, ***247V***, ***254S***, ***255A***, ***258G***, ***259I***, ***260A***, ***261V***, ***262L***, ***263D***.
Oxy-hemoglobin-nsp9 complex	-26.06	**Chain A** ***78D***, ***79T***, ***80P***, ***107A***, ***108A***, ***109T***, ***110V***, ***111R***. **Chain B** ***9L***, ***10R***, ***11Q***, ***12M***, ***13S***, ***29L***, ***31Y***, ***32Y***, 34T, 35T, 36K, 37G, 38G, ***39R***, ***45L***,***57P***, ***58K***,***59S***, ***60D***, ***61G***, 62T, ***107A***, ***108A***, ***109T***, ***110V***, ***111R***.
Oxy-hemoglobin-nsp16-nsp10 complex	-55.88	**Chain A (nsp16)** 30Y, 33S,34A, 35T, 36L, 37P, 38K, 39G, 40I, 42M, 75D, 76K. **Chain B (nsp10)** ***19F***, ***20A***, ***21V***, 22D, 23A, 25K, 26A, 27Y, 28K, 29D, 30Y, 31L, 33S, 34G, 35G, 36Q, 37P, 39T, 40N, 43K, 66E, ***79C***, ***80H***, ***81I***, ***82D***, 101T, 104A, 105N.
Deoxyhemoglobin-nsp5 complex	-42.09	**Chain A** ***48D***, ***50L***, ***51N***, 52P, ***53N***, ***56D***, 57L, ***60R***, ***188R***, ***190T***, ***191A*** **Chain B** ***154Y***, 209Y, 212V, 213I, 217R,***247V***, ***248D***, ***249I***, ***251G***, ***252P***, ***253L***, ***254S***, ***255A***, ***256Q***, ***257T***, ***258G***, ***294F***, ***297V***, ***301S***, ***302G.*** **Chain C** ***19Q***, ***21T***, ***23G***, ***24T***,***25T***, ***26T***, 27L, ***46S***, ***47E***, 49M, 69Q, ***118Y***, ***119N***, ***142N***, 143G, 189Q.
Deoxyhemoglobin-nsp9 complex	-26.59	**Chain A** 12N, ***13S***, 14C, 15A, 16A, 19T, 20Q, 21T, 22A, 23C, 24T, 25D, 26D, 27N, 39R, 48L, 50D,53W, 55A,56F, 57P, 58K, 59S, 60D,61G, 62T, 63G, 64T, 66Y
Deoxyhemoglobin-nsp16-nsp10 complex	-44.07	**Chain A (nsp16)** ***102D***, ***103F***, ***108D***, ***110T***, ***111L***, ***112I***, ***113G***,119H, 120T, 121A, 160K, ***286N***, ***287R***, ***288V***, ***289V***, ***291S***, ***292S***, 293D, 294V, 295L, 296V, 297N. **Chain B (nsp10)** 76Y, 80H, 81I, 82D, 83H, 86P, 87K, 88G, ***89F***, 90C, 93K.

The blue, red, and orange colored residues referred to the amino acid residues in the nsp-MRJP2, nsp-MRJP2 X1, or both, respectively that matched the binding site residues of nsp-hemoglobin complex. SARS-CoV-2, severe acute respiratory syndrome-related coronavirus; nsps, non-structural proteins.

binding pocket residues in the studied docked complexes revealed the possibility for a competitive inhibitory effect of RJ proteins. No matching residues were detected with ACE2 active sites in either of the studied complexes, ACE2-MRJP2 or ACE2-MRJP2 X1. However, after examination of the binding pocket in the ACE2-inhibitor complex (PDB: IR42), the results showed a matching residue with the ACE2-MRJP2 (D615) and ACE2-MRJP2 X1 (P135) binding sites (Fig. S2 Iii, IIii). Moreover, analysis using Discovery Studio software revealed that the binding residues in ACE2-RBD complex (PDB: 6M0J) did not match any of the binding residues between MRJP2 or its isoform X1 and ACE2 (Fig. S2 I, II). However, they matched certain binding residues in RBD-MRJP2 (G446, Y449, E484, Fig. S2 IIIii) and RBD-MRJP2 X1 (G446, T500, Fig. S2 IVii).

The data showed that MRJP2 can attach to certain active site residues in nsp3, nsp5, and nsp9 only and cannot bind to the active site residues of the other studied nsps (Fig. 2 Iii, 4 IIIii, 5 Iii). After comparing the binding residues in the nsp3-inhibitor complex (PDB: 6WUU) with the binding pocket in the nsp3-MRJP2 via the Discovery Studio software, some matching residues were detected. These residues included P247B, P248B, Y268B, G163D, D164D, P247D, P248D, Y264D, N267D, Y268D, and Y273D (Fig. 2 Iii). Moreover, some of the amino acid residues in the binding site of the nsp5-MRJP2 complex matched the binding residues in the nsp5-inhibitor complex (PDB: 7BRP), including P168A, R188A, Q189A, T190A, A191A, and Q192A (Fig. 2 IIIii). However, no matching residues were detected with the analyzed nsp12- and nsp16-inhibitor complexes (PDB: 7BV2 and 6YZ1, respectively). The data also revealed that MRJP2 can interact with various nsp7-nsp8 cofactors-binding residues in nsp12, including L270, P323,

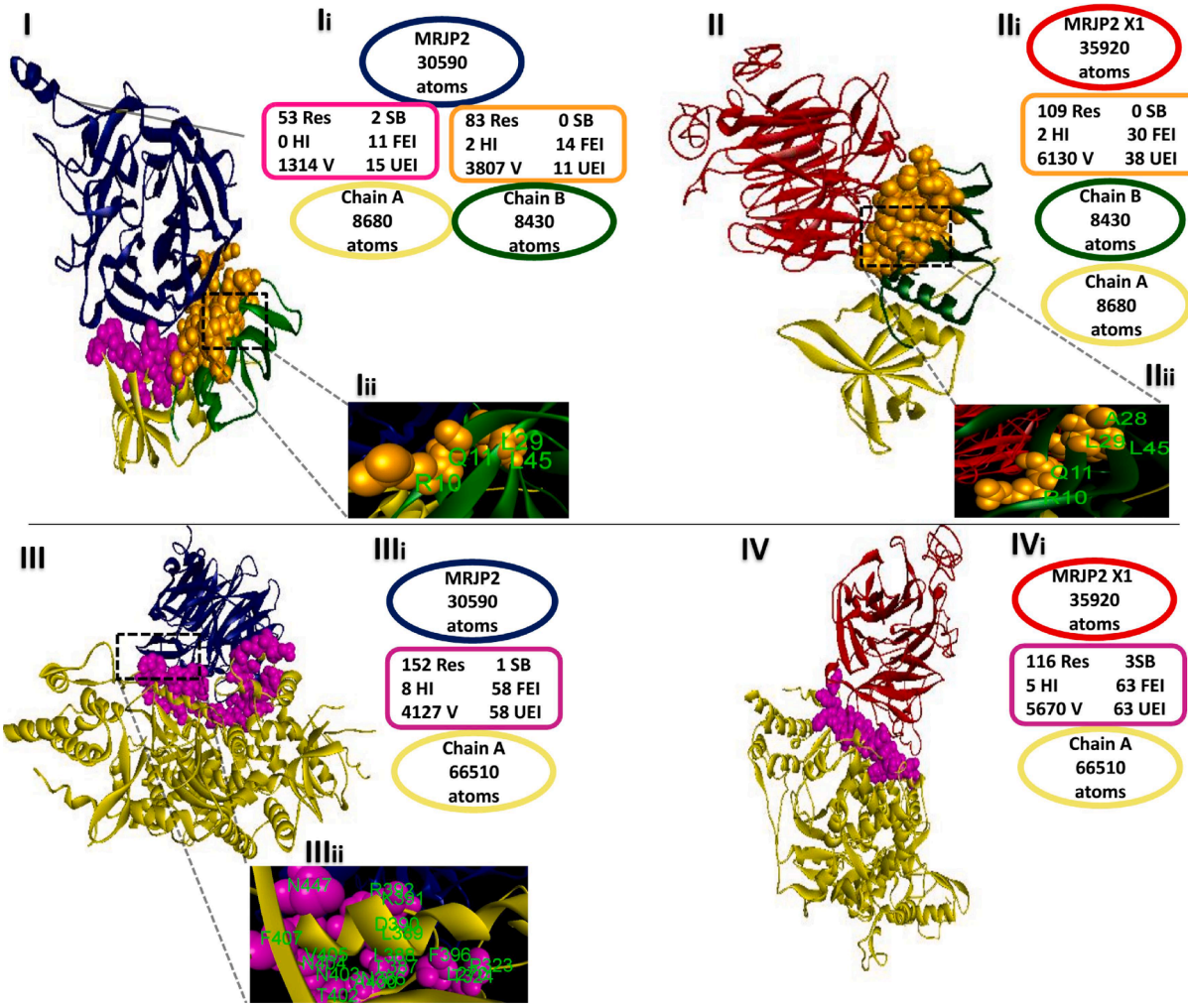

Fig. 3. Molecular docking analysis of MRJP2 and MRJP2 isoform X1 with the SARS-CoV-2 nsp9 and nsp12. ***(I, II)*** Docking models of MRJP2 (shown in blue) and MRJP2 X1 (shown in red), respectively with nsp9 (PDB: 6WXD, shown in yellow chain A, green chain B). ***(III, IV)*** Docking models of MRJP2 (shown in blue) and MRJP2 X1 (shown in red), respectively with nsp12 (PDB: 7BV2, chain A, shown in yellow). The amino acid residues with the space-filling spheres style (shown in pink chain A, orange chain B) indicate the binding residues in the docked complexes. ***(Ii-IVi)*** Illustrations of the interchain interactions (rectangle shapes) in the docked complexes. ***(Iii-IIii)*** Magnification of nsp9′s active site amino acid residues that can bind with MRJPs. ***(IIIii)*** Magnification of nsp12′s cofactor (nsp7-nsp8)-binding amino acid residues that can interact with MRJP2. ***Res*** – residues, ***HI*** – hydrophobic interaction, ***V*** – van der Waals, ***SB*** – salt bridge, ***FEI*** – favorable electrostatic interaction, ***UEI*** – unfavorable electrostatic interaction. (For interpretation of the references to colour in this figure legend, the reader is referred to the web version of this article.)

T324, N386, L387, L388, L389, D390, K391, R392, F396, A400, T402, N403, N404, V405, F407, and N447 (Fig. 3 IIIii). Likewise, it can bind to some residues in nsp16 that are specific to the binding of the nsp10 cofactor, these residues include R86, D102, V104, S105, D106, A107, and T110 (Fig. S4 Iii). On the other hand, MRJP2 X1 formed a complex at certain active site residues in the nsp3, nsp5, nsp9, and nsp16 (Fig. 2 IIii, 4 IVii, 5 IIii, 7 IIii). Also, one (R188A) matching residue was detected at the binding site of the nsp5-MRJP2 X1 complex with nsp5-inhibitor (Fig. 2 IVii) and several (N13A, T56A, L57A, T58A, W189A, and C209A) residues were found at its binding site with the nsp16-inhibitor (Fig. S4 IIii) complex. However, no matching residues were detected with the studied nsp3-inhibitor and nsp12-inhibitor complexes. Similarly, no matching residues were detected at the binding sites of nsp12-MRJP2 X1 and nsp16-MRJP2 X1 docked complexes with nsp12 active site residues or cofactors and nsp16-cofactor complex binding residues, respectively. Matching residues between the studied complexes and the nsp9-inhibitor complex were not studied due to the unavailability of this inhibitor complex in the PDB database at the time of study.

Concerning the binding of nsp5, nsp9, or nsp16-nsp10 to oxy- and deoxyhemoglobin, various matching residues with the binding site in the respective nsp-MRJP docked complexes were detected (Table 1).

4. Discussion

The *A. mellifera* RJ is an important functional food comprising nine MRJPs with many reported activities. The two proteins, MRJP2 and its isoform X1, were purified as previously elucidated (Abu-Serie & Habashy, 2019), and their 3D structures were generated using the I-TASSER web server. Various functions for these two purified RJ proteins, including sialidase activity, have been predicted from the COFACTOR and COACH servers. Therefore, the current study evaluated this predicted activity practically, and the results confirmed it. Sialidases [neuraminidases, EC 3.2.1.18] control cellular activity by removing SA from endogenous glycoconjugates. This effect can influence various cell activities, such as cell adhesion, signaling, and apoptosis (Schwerdtfeger, Melzig, & Melzig, 2010). SA is a nine-carbon monosaccharide molecule that always occupies the terminal position of glycoproteins and glycolipid oligosaccharide chains in all cell types (Varki, 2008; Zhang, Chen, Liu, & Xu, 2019). It can interact through α2,3 or α2,6

glycosidic linkage to Gal/GalNAc or via α2,8 linkage to another SA by a group of sialyltransferases (Cohen & Varki, 2010). SA plays a crucial role in various essential pathological processes, such as cancer metastases, viral, bacterial, and parasite infection, in addition to certain physiological processes (Varki, 2008; Zhang et al., 2019). Hence, it serves as a receptor for some viruses, such as influenza A (swine – H1N1, avian – H5N1) (Chu & Whittaker, 2004) and C (Varki, 2008), β-coronaviruses (Tortorici et al., 2019), human adenovirus, reovirus, human picornavirus (coxsackievirus A24 variant, enterovirus 68, and enterovirus 70), and polyomavirus. These viruses interact with other particular cell surface receptors besides SA in a certain sequential fashion, where the initial attachment primes the viral structure to interact with specific receptors (Blaum & Stehle, 2019). In addition, some bacteria (*Helicobacter pylori*), bacterial toxins (*Vibrio cholerae* and *Clostridium botulinum*), and parasites (*Plasmodium falciparum*) require SA to invade host cells (Varki, 2008). In the current study, WI-38 cells were used to study the sialidase activity of MRJP2 and MRJP2 X1. Here, we considered this cell type due to the fact that lung cells are the most susceptible to SARS-CoV-2 infection (Chan et al., 2020). The presence of SA on the surface of these cells has already been confirmed (Itakura et al., 2016). Based on the EC50 values (Fig. 1 Ii and IIi), the MRJP2 was observed to have more potent sialidase activity than MRJP2 X1. In addition, a combination study of both purified RJ proteins as PF_{50} showed synergistic activity (CI < 1) after 2 h and 72 h of incubation with WI-38. Therefore, it can be inferred that the PF_{50} possesses a stronger sialidase activity than the individual proteins. The present study performed a molecular docking analysis for each of the tested RJ proteins with NeuAc and 9-O-Ac-SA to identify interacting residues and predict active sites. NeuAc and 9-O-Ac-SA were selected because the former is the most popular type of SA targeted by mammalian and human pathogens (Blaum & Stehle, 2019; Varki, 2008), and the latter is vital for the entry of β-CoV (Tortorici et al., 2019). Docking results showed that the two studied proteins were capable of interacting with either NeuAc or 9-O-Ac-SA with different types of interactions (Fig. S1). Based on the ACEV and fullfitness values, the binding affinity of MRJP2 to NeuAc and 9-O-Ac-SA was found to be nearly the same but higher than MRJP2 X1, while the binding affinity of MRJP2 X1 to NeuAc was higher than that of 9-O-Ac-SA. This may be related to the difference in the number and type of non-covalent interactions with the two analyzed SA forms. In fact, the presence of electrostatic interactions, mainly hydrogen bonds, in the docked complex contributes to its binding stability and affinity. The ability of our tested RJ proteins to hydrolyze SA from the surface of the cells would the block uptake of and, in turn, infection with various viruses, bacteria, bacterial toxins, and parasites. This reflects the broad-spectrum antipathogenic function of our studied proteins. Hence, it can be concluded that β-CoVs need 9-O-Ac-SA to enter host cells (Tortorici et al., 2019), and since SARS-CoV-2 is classified as one of this genus (Letko & Munster, 2020), it may also depend on SA for cell entry. This suggestion was recently confirmed via various modelling studies (Fantini, Di Scala, Chahinian, & Yahi, 2020; Robson, 2020). Therefore, the release of SA from the cell surface via MRJPs may interfere with the entry of this virus. Following this result, the antiviral drug chloroquine gave positive results against SARS-CoV-2 due to its ability to prevent sialic acid synthesis (Xu et al., 2020).

All CoVs can interact with the host cell receptor through the spike fusion peptide and are released by the adjacent host protease to allow virus entry (Simmons, Zmora, Gierer, Heurich, & Pöhlmann, 2013). The identified receptor for SARS-CoV is ACE2 (Li et al., 2003), which has recently been reported to be the receptor for SARS-CoV-2 (Letko & Munster, 2020). The present study evaluated the impact of MRJP2 and its isoform on the ACE2 and RBD S1 domain using a set of computational methods. These proteins were able to bind to ACE2. The docking analysis revealed that MRJP2 and its isoform X1 were able to interact individually with human ACE2 via different non-covalent interactions, and the binding energies were −47.98 and −33.24, respectively. Meanwhile, the stability of MRJP2′s binding to ACE2 was more than that of MRJP2 X1. No matching residues were found after examination of the binding residues between ACE2 and MRJP2 or MRJP2 X1 with the active site residues of the enzyme. Therefore, the tested RJ proteins did not have a competitive inhibitory effect on ACE2, but they may or may not inhibit its activity via other mechanisms. Hence the binding residues between ACE2 and MRJP2 or MRJP2 X1 matched the binding residues in the ACE2-inhibitor complex (PDB: IR42) at D615 and P135, respectively. Also, MRJP2 and its isoform X1 could bind to viral RBD with different binding energies (−48.12 and −51.12 Kcal/Mol, respectively). We found that the binding residues in the ACE2-RBD complex (PDB: 6m0J) did not match any of the binding residues between ACE2 and MRJPs, although they matched some residues at the site of RBD's binding to MRJP2 (G446, Y449, E484) or to MRJP2 X1 (G446, T500). Such findings have shown that MRJP2 and its isoform X1 may not be able to block the viral binding site on the ACE2 receptor, but may block the viral surface and diminish its receptor attachment ability. These outcomes were in line with our recently published results that proved the ability of these functional food proteins to block the entry of HCV and HBV into their host cells (Habashy & Abu-Serie, 2019).

The current study used a set of computational analyses with different computational tools to evaluate the impact of MRJP2 and MRJP2 X1 on different viral enzymes, including nsp3, nsp5, nsp9, nsp12, and nsp16. We focused on evaluating these viral proteins in an attempt to develop an effective drug for this serious viral infection. Hence, these proteins have been proposed here as viable targets for anti-SARS-CoV-2 drugs. The nsp3 is the largest nsp (~1945 aa) with 3 cleavage sites in the N-terminal part of the polyprotein 1a and 1ab for releasing nsp1, nsp2, and nsp3. Also, it can interact with other nsps such as nsp4 and nsp6 for viral replication, in addition to its ability to bind to structural and host proteins as a scaffold. Besides its nsps maturation capability, the nsp5 (~306 aa) has 11 distinct cleavage sites on polyproteins 1a and 1ab to release nsp4-nsp16, while nsp9 (~113 aa) can bind to single-stranded RNA in a dimeric form—which is important for viral replication. RNA-dependent RNA polymerase (nsp12, ~932 aa) is a very important viral protein and participates in viral genome replication and transcription. This protein must interact with nsp7-nsp8 cofactors to stabilize and extend its RNA-binding surface. The nsp16 (~298 aa) encodes 2′-O-methyltransferase, which is responsible for RNA cap methylation at ribose 2′-O positions, thereby producing a cap-1 structure. The activity of this protein and its binding to its substrate needs nsp10 as a cofactor (Qiu & Xu, 2020). The molecular docking results showed different energies for the binding of MRJP2 and its isoform X1 to the studied viral enzymes, indicating the different binding affinity of the two proteins. MRJP2 had a good affinity to certain residues in the active site pocket of nsp3, nsp5, and nsp9, while MRJP2 X1 displayed certain interactions with various amino acid residues at the active sites of these viral enzymes in addition to nsp16 (Table 1, Figs. 2, 3, S3, and S4). Therefore, these RJ proteins may act as competitive inhibitors for these viral enzymes. In addition, this study examined the nsp7-nsp8 and nsp10 critical binding residues in nsp12 and nsp16, respectively, using nsp12-nsp7-nsp8 and nsp16-nsp10 complex templates (PDB: 7BV2 and 6YZ1, respectively). Data revealed that MRJP2—but not MRJP2 X1—can interact with many of the nsp7-nsp8 and nsp10 binding residues. Therefore, the binding of MRJP2 to nsp12 or nsp16 prevents the interaction of their cofactors and inhibits their activities, which in turn stops viral replication, as nsp12-nsp7-nsp8 and nsp16-nsp10 complexes are necessary structures for viral replication (Qiu & Xu, 2020). In addition, a comparison between the binding residues of the nsp-inhibitor complex and those of the MRJP2 and MRJP2 X1 docked complexes showed some similar residues. Thus, MRJP2 and MRJP2 X1 may be supposed to be good inhibitors of the examined SARS-CoV-2 enzymes.

Besides the role of nsps in viral replication, they help the virus evade host cell immunity. Hence the nsp5 overwhelms innate immune responses (IFN-stimulated genes) via proteolytic digestion of the vital enzymes in the immune signal transduction pathway. Moreover, the cap-1 type of modification that occurred via nsp16 helps SARS-CoV-2 to

escape from the RNA recognition system and the IFN-I mediated antiviral responses—the host cell antiviral sensors (Qiu & Xu, 2020). Thus, this inhibitory effect on nsp5 and nsp16 activities by the tested RJ proteins not only suppresses viral replication but may also increase the sensitivity of the host cells to innate immunity for viral detection after entry. Otherwise, it was reported that nsp5, nsp9, and nsp16-nsp10 can bind to porphyrin and attack the heme on oxy- and deoxyhemoglobin. The present study agrees with this outcome; hence the molecular docking revealed the binding of these nsps to both forms of hemoglobin (Fig. S5). Hemoglobin attacks can occur after hemolysis of the red blood cells (RBCs) as a result of their membrane rupture by the virus or after its infection via the spike-CD147 pathway or other mechanisms. The virus can also infect the plasma cells; then the viral proteins reach the blood and attack hemoglobin during the antibodies secretion (Wang et al., 2020). Binding viral proteins to hemoglobin will inhibit its correctly folding structure and, in turn, disrupt and release heme and iron into the blood. This damage effect reduces the ability of the blood to carry oxygen, leading to hypoxia, which in turn elevates the inflammatory cytokines (IL-1 and TNF-α), hyaluronic acid content, and enhances blood thrombosis in the lung. In addition, the elevation of free iron in the blood will induce oxidative stress, resulting in more hemolysis and further oxidative stress, hypoxia, and thrombosis (Joly, Siguret, & Veyradier, 2020; Lavranos, 2020). Thus, the ability of the MRJP2 and its isoform to bind to the nsps at the same hemoglobin-binding site can affect their attachment. Additionally, the current study examined the binding affinity between these nsps and hemoglobin and compared it with the corresponding values of the tested MRJPs. The results showed higher affinity for nsp5, nsp9, and nsp16-nsp10 to both studied MRJPs, or to MRJP2 only or to MRJP2 isoform X1 only, respectively (Table 1). This result boosts the prediction of the MRJPs' ability to prevent nsps–hemoglobin interaction. Thus, these MRJPs will be able to prohibit hypoxia and its pathogenesis, particularly inflammation and thrombosis. These findings signify the importance of RJ proteins in preventing not only viral replication but also its serious complications.

5. Conclusions

The protein–protein interaction plays a crucial role in structure-based drug designing. This study provides insights into the interactions of MRJP2 and its isoform X1 with the vital proteins of SARS-CoV-2. These two functional food proteins are supposed to be efficient in preventing SARS-CoV-2 cell-attachment due to their sialidase activity and their ability to interact with the ACE2 binding sites on the viral spike RBD. Based on the docking analysis, these RJ proteins can bind to the active site or cofactor-binding site residues on the viral nsp3, nsp5, nsp9, nsp12, and nsp16, thus inhibiting their activities. In addition, these proteins may prevent viral complications in the lung, such as hypoxia and its pathogenesis, due to their ability to efficiently bind to most of the oxy- and deoxyhemoglobin binding sites on the viral nsps. Therefore, MRJP2 and MRJP2 isoform X1 represent a hope of eliminating this deadly virus that has been spreading at an alarming rate.

The obtained results suggest specific potency and mechanisms for each of these RJ proteins. In this context, the authors predict the use of both proteins together (PF_{50})— than individually—to have more efficacy against SARS-CoV-2. However, further investigations, like *in vitro* testing on the real virus and its proteins, are still required to confirm these predicted mechanisms.

Funding

This research did not receive any specific grant from funding agencies in the public, commercial, or not-for-profit sectors.

Author contributions

N.H.H and M.M.A have equally contributed to designing and accomplishing the experiments, analyzing and interpreting the results as well as writing and revising the manuscript.

Ethical statement

This research did not include any human subjects and animal experiments.

CRediT authorship contribution statement

Noha H. Habashy: Conceptualization, Writing - original draft, Writing - review & editing, Software, Data curation, Validation, Visualization. **Marwa M. Abu-Serie:** Methodology, Writing - review & editing, Software, Data curation, Validation, Visualization.

Declaration of Competing Interest

The authors declare that they have no known competing financial interests or personal relationships that could have appeared to influence the work reported in this paper.

The authors filed a Patent Cooperation Treaty (PCT, Application number: PCT/EG2018/000012, International Filing Date: 6 Dec. 2018, Publication Date: 18 Oct. 2018) with respect to the topic of sialidase activity and anti-coronavirus efficacy of RJ proteins.

Appendix A. Supplementary material

Supplementary data to this article can be found online at https://doi.org/10.1016/j.jff.2020.104282.

References

Abu-Serie, M. M., & Habashy, N. H. (2019). Two purified proteins from royal jelly with in vitro dual anti-hepatic damage potency: Major royal jelly protein 2 and its novel isoform X1. *International Journal of Biological Macromolecules, 128*, 782–795.

Ahmad, S., Campos, M. G., Fratini, F., Altaye, S. Z., & Li, J. (2020). New insights into the biological and pharmaceutical properties of royal jelly. *International Journal of Molecular Sciences, 21*, 382–407.

Albert, S., Bhattacharya, D., Klaudiny, J., Schmitzová, J., & Simúth, J. (1999). The family of major royal jelly proteins and its evolution. *Journal of Molecular Evolution, 49*(2), 290–297.

Aminoff, D. (1961). Methods for the quantitative estimation of N-acetylneuraminic acid and their application to hydrolysates of sialomucoids. *Biochemical Journal, 81*(2), 384–392.

Bassetti, M., Vena, A., & Giacobbe, D. R. (2020). The novel Chinese coronavirus (2019-nCoV) infections: Challenges for fighting the storm. *European Journal of Clinical Investigation, 50*(3), e13209–e13213.

Blaum, B. S., & Stehle, T. (2019). Sialic acids in nonenveloped virus infections. *Advances in Carbohydrate Chemistry and Biochemistry, 76*, 65–111.

Bradford, M. M. (1976). A rapid and sensitive method for the quantitation of microgram quantities of protein utilizing the principle of protein-dye binding. *Analytical Biochemistry, 72*, 248–254.

Chan, J. F. W., Kok, K. H., Zhu, Z., Chu, H., To, K. K. W., Yuan, S., & Yuen, K. Y. (2020). Genomic characterization of the 2019 novel human-pathogenic coronavirus isolated from a patient with atypical pneumonia after visiting Wuhan. *Emerging Microbes & Infections, 9*(1), 221–236.

Chen, Y., Liu, Q., & Guo, D. (2020). Emerging coronaviruses: Genome structure, replication, and pathogenesis. *Journal of Medical Virology, 92*(4), 418–423.

Chinese Center for Disease Control and Prevention (2020). Epidemic update and rsk assessment of 2019 novel coronavirus. pp. 1–11.

Chou, T. C. (2006). Theoretical basis, experimental design, and computerized simulation of synergism and antagonism in drug combination studies. *Pharmacological Reviews, 58*(3), 621–681.

Chu, V. C., & Whittaker, G. R. (2004). Influenza virus entry and infection require host cell N-linked glycoprotein. *Proceedings of the National Academy of Sciences of the United States of America, 101*(52), 18153–18158.

Cohen, M., & Varki, A. (2010). The sialome-far more than the sum of its parts. *OMICS: A Journal of Integrative Biology, 14*(4), 455–464.

Cui, J., Li, F., & Shi, Z. L. (2019). Origin and evolution of pathogenic coronaviruses. *Nature Reviews Microbiology, 17*(3), 181–192.

EL-Fiky, S., Abu-Serie, M., & Habashy, N. (2018). Anti-leukemic, anti-HIV, and sialidase activities of royal-jelly proteins. Patentscope, PCT/EG2018/000012, WO/2018/188714.

EL-Fiky, S., Abu-Serie, M., & Habashy, N. (2020). Antiviral, antifibrotic and anticancer activities of royal-jelly proteins. United States Patent and Trademark Office, US 20200207820.

Elfiky, A. A. (2020). Ribavirin, Remdesivir, Sofosbuvir, Galidesivir, and Tenofovir against SARS-CoV-2 RNA dependent RNA polymerase (RdRp): A molecular docking study. *Life Sciences, 253*, 117592–117597.
Fantini, J., Di Scala, C., Chahinian, H., & Yahi, N. (2020). Structural and molecular modelling studies reveal a new mechanism of action of chloroquine and hydroxychloroquine against SARS-CoV-2 infection. *International Journal of Antimicrobial Agents., 55*(5), 105960–105967.
Fratini, F., Cilia, G., Mancini, S., & Felicioli, A. (2016). Royal Jelly: An ancient remedy with remarkable antibacterial properties. *Microbiological Research, 192*, 130–141.
Gorbalenya, A. E. (2020). Severe acute respiratory syndrome-related coronavirus – The species and its viruses, a statement of the Coronavirus Study Group. *BioRxiv*, 1–15.
Grosdidier, A., Zoete, V., & Michielin, O. (2011). SwissDock, a protein-small molecule docking web service based on EADock DSS. *Nucleic Acids Research, 39*, W270–W277.
Habashy, N. H., & Abu-Serie, M. M. (2019). Major royal-jelly protein 2 and its isoform X1 are two novel safe inhibitors for hepatitis C and B viral entry and replication. *International Journal of Biological Macromolecules, 141*, 1072–1087.
Itakura, Y., Sasaki, N., Kami, D., Gojo, S., Umezawa, A., & Toyoda, M. (2016). N- and O-glycan cell surface protein modifications associated with cellular senescence and human aging. *Cell & Bioscience, 16*(14), 1–11.
Joly, B. S., Siguret, V., & Veyradier, A. (2020). Understanding pathophysiology of hemostasis disorders in critically ill patients with COVID-19. *Intensive Care Medicine, 46*(8), 1603–1606.
Laskowski, R. A., Jabłońska, J., Pravda, L., Vařeková, R. S., & Thornton, J. M. (2018). PDBsum: Structural summaries of PDB entries. *Protein Science, 27*(1), 129–134.
Lavranos, G. (2020). The role of blood disorders in the manifestation of ARDS in COVID 19 and EPO as a potential therapeutic agent. *Qeios*.
Letko, M., & Munster, V. (2020). Functional assessment of cell entry and receptor usage for lineage B β-coronaviruses, including 2019-nCoV. *Nature Microbiology, 5*(4), 562–569.
Li, G., Fan, Y., Lai, Y., Han, T., Li, Z., Zhou, P., … Wu, J. (2020). Coronavirus infections and immune responses. *Journal of Medical Virology, 92*(4), 424–432.
Li, W., Moore, M. J., Vasllieva, N., Sui, J., Wong, S. K., Berne, M. A., … Farzan, M. (2003). Angiotensin-converting enzyme 2 is a functional receptor for the SARS coronavirus. *Nature, 426*(6965), 450–454.
Mashiach, E., Schneidman-Duhovny, D., Andrusier, N., Nussinov, R., & Wolfson, H. J. (2008). FireDock: A web server for fast interaction refinement in molecular docking. *Nucleic Acids Research, 36*(suppl_2), W229–W232.
Mathew, O., & Sowdhamini, R. (2016). PIMA: Protein-protein interactions in macromolecular assembly – A web server for its analysis and visualization. *Bioinformation, 12*(1), 9–11.
Mosmann, T. (1983). Rapid colorimetric assay for cellular growth and survival: Application to proliferation and cytotoxicity assays. *Journal of Immunological Methods, 65*(1–2), 55–63.
Qiu, Y., & Xu, K. (2020). Functional studies of the coronavirus nonstructural proteins. *STEMedicine, 1*(2), e39.
Robson, B. (2020). Bioinformatics studies on a function of the SARS-CoV-2 spike glycoprotein as the binding of host sialic acid glycans. *Computers in Biology and Medicine, 122*, 103849–103866.
Salentin, S., Schreiber, S., Haupt, V. J., Adasme, M. F., & Schroeder, M. (2015). PLIP: Fully automated protein-ligand interaction profiler. *Nucleic Acids Research, 43*(W1), W443–W447.
Scarselli, R., Donadio, E., Giuffrida, M. G., Fortunato, D., Conti, A., Balestreri, E., … Felicioli, A. (2005). Towards royal jelly proteome. *Proteomics, 5*, 769–776.
Schneidman-Duhovny, D., Inbar, Y., Nussinov, R., & Wolfson, H. J. (2005). PatchDock and SymmDock: Servers for rigid and symmetric docking. *Nucleic Acids Research, 33*, W363–W367.
Schwerdtfeger, S. M., Melzig, M. F., & Melzig, M. M. (2010). Sialidases in biological systems. *Pharmazie, 65*(8), 551–561.
Simmons, G., Zmora, P., Gierer, S., Heurich, A., & Pöhlmann, S. (2013). Proteolytic activation of the SARS-coronavirus spike protein: Cutting enzymes at the cutting edge of antiviral research. *Antiviral Research, 100*(3), 605–614.
Šimúth, J., Bíliková, K., Kováčová, E., Kuzmová, Z., & Schroder, W. (2004). Immunochemical approach to detection of adulteration in honey: Physiologically active royal jelly protein stimulating TNF-α release is a regular component of honey. *Journal of Agricultural and Food Chemistry, 52*(8), 2154–2158.
Tok, T. T., & Tatar, G. (2017). Structures and functions of coronavirus proteins: Molecular modeling of viral nucleoprotein. *International Journal of Virology & Infectious Diseases, 2*(1), 1–7.
Tortorici, M. A., Walls, A. C., Lang, Y., Wang, C., Li, Z., Koerhuis, D., … Veesler, D. (2019). Structural basis for human coronavirus attachment to sialic acid receptors. *Nature Structural & Molecular Biology, 26*(6), 481–489.
Tovchigrechko, A., & Vakser, I. A. (2006). GRAMM-X public web server for protein-protein docking. *Nucleic Acids Research, 34*, W310–W314.
Varki, A. (2008). Sialic acids in human health and disease. *Trends in Molecular Medicine, 14*(8), 351–360.
Wang, X., Xu, W., Hu, G., Xia, S., Sun, Z., Liu, Z., … Lu, L. (2020). SARS-CoV-2 infects T lymphocytes through its spike protein-mediated membrane fusion. *Cellular and Molecular Immunology*, 1–3.
WHO (2004). Summary of probable SARS cases with onset of illness from 1 November 2002 to 31 July 2003. Online 2004.
WHO (2019). WHO MERS-CoV Global Summary and Assessment of Risk, July 2019 (WHO/MERS/RA/19.1). July, 1–10.
WHO (2020). Coronavirus disease 2019. 2019 (March), 2633. https://www.who.int/emergencies/diseases/novel-coronavirus-2019.
Xu, Z., Peng, C., Shi, Y., Zhu, Z., Mu, K., Wang, X., & Zhu, W. (2020). Nelfinavir was predicted to be a potential inhibitor of 2019-nCov main protease by an integrative approach combining homology modelling, molecular docking and binding free energy calculation. *BioRxiv*.
Yang, J., Roy, A., & Zhang, Y. (2013). Protein-ligand binding site recognition using complementary binding-specific substructure comparison and sequence profile alignment. *Bioinformatics, 29*(20), 2588–2595.
Yang, J., & Zhang, Y. (2015). I-TASSER server: New development for protein structure and function predictions. *Nucleic Acids Research, 43*(W1), W174–W181.
Zhang, C., Chen, J., Liu, Y., & Xu, D. (2019). Sialic acid metabolism as a potential therapeutic target of atherosclerosis. *Lipids In Health and Disease, 18*(1), 173.
Zhang, C., Freddolino, P. L., & Zhang, Y. (2017). COFACTOR: Improved protein function prediction by combining structure, sequence and protein-protein interaction information. *Nucleic Acids Research, 45*(W1), W291–W299.